Idealized Particle-Resolved Large-Eddy Simulations to Evaluate the Impact of Emissions Spatial Heterogeneity on CCN Activity

Samuel Frederick[1], Matin Mohebalhojeh[2], Jeffrey Curtis[1,2], Matthew West[2], and Nicole Riemer[1]

[1]Department of Climate, Meteorology, and Atmospheric Sciences, University of Illinois Urbana–Champaign, 105 S Gregory St., Urbana, IL 61801, USA
[2]Department of Mechanical Science and Engineering, University of Illinois Urbana–Champaign, 1206 W. Green St., Urbana, IL, 61801,USA

Correspondence: Nicole Riemer (nriemer@illinois.edu)

Abstract. Aerosol-cloud interactions remain a large source of uncertainty in global climate models (GCMs) due to complex, nonlinear processes that alter aerosol properties and the inability to represent the full compositional complexity of aerosol populations within large-scale modeling frameworks. The spatial resolution of GCMs is often coarser than the scale of the spatially varying emissions in the modeled geographic region. This results in diffuse, uniform concentration fields of primary aerosol and gas-phase species instead of spatially heterogeneous concentrations. Aerosol processes such as gas-particle partitioning and coagulation are concentration-dependent in a non-linear manner, and thus the representation of spatially heterogeneous emissions impacts aerosol aging and properties. This includes climate-relevant quantities key to aerosol-cloud interactions including particle hygroscopicity and cloud condensation nuclei (CCN) activity. We investigate the impact of emissions spatial heterogeneity on aerosol properties including CCN activity via a series of first-of-a-kind particle-resolved large-eddy simulations with the modeling framework WRF-PartMC-MOSAIC-LES. CCN concentrations within the planetary boundary layer (PBL) are compared across numerous scenarios ranging in emissions spatial heterogeneity. We find that CCN concentrations at low supersaturations ($S = 0.1$–0.3%) increase in the upper PBL by up to 25% for emissions scenarios with high spatial heterogeneity when compared to a uniform emissions base case.

1 Introduction

Aerosols are known to impose a net negative radiative forcing, however considerable uncertainty persists in the representation of radiative forcing due to aerosol-cloud interactions (ACI) (Forster et al., 2021). Advancements in computing power have allowed modelers to investigate key contributing factors which alter the intensity of radiative forcing due to ACI such as spatial resolution (Ma et al., 2015). Simultaneously, improvements in computational power have advanced the representation of aerosols in climate models through inclusion of more complex chemical mechanisms (citation?) and detailed aerosol treatments such as the Community Aerosol and Radiation Model for Atmospheres (CARMA) , which is a 40 bin sectional model used by the Community Earth System Model 2 (CESM2) (Tilmes et al., 2023) and has shown improvements in representing aerosol properties when compared to the 4 bin Modal Aerosol Model (MAM4). While these two key structural components to models—the treatment of aerosols and the effect of spatial resolution—have improved representation of aerosols and their radiative

forcing, these aspects have yet to be explored in tandem to investigate the role of spatial heterogeneities typically below the grid scale of current climate models alongside detailed aerosol treatments in modifying the depiction of climate-relevant aerosol properties key to ACI such as cloud condensation nuclei (CCN) activity.

Aerosol-aware climate models typically contain a sub-model which governs the aerosol representation and associated processes. Given computational constraints, the aerosol treatment is often highly simplified with regard to aerosol compositional diversity. For instance, E3SM uses the modal aerosol model MAM4 which contains four lognormally distributed modes Golaz et al. (2022). Such a treatment constrains the diversity of the aerosol population to four internally-mixed modes (i.e., all particles within a mode are compositionally identical). As a result, modal and sectional aerosol treatments underrepresent the true compositional complexity of an aerosol population in which each particle ages independently. Particle-resolved aerosol models allow representation of the full compositional diversity of an aerosol population via a set of computational particles which are allowed to compositionally vary and age independently. Particle resolved models such as the Particle Monte Carlo model (PartMC) have been used extensively to investigate the sensitivity of CCN activity to the composition of emitted aerosol particles (Fierce et al., 2013), aging timescales due to condensation and coagulation for carbonaceous CCN (Fierce et al., 2015), and the sensitivity of CCN estimates to mixing state (i.e., the compositional diversity within and across aerosols) (Ching et al., 2017). Furthermore, given that a particle-resolved model can fully represent aerosol composition space, PartMC has been used to estimate error in CCN activity for coarser aerosol treatments by comparing depicted CCN concentrations against compositionally-averaged output reminiscent of a sectional or modal model (Zaveri et al., 2010; Ching et al., 2017). Furthermore, direct comparison of CCN activity depicted by PartMC and MAM4 has shown considerable divergence, especially in polluted regions where high rates of coagulation and gas-particle partitioning amplify model disagreement (Fierce et al., 2024).

In addition to the treatment of aerosols, the depiction of spatial heterogeneity—including that of surface properties, emissions of gas phase species and primary aerosol, and heterogeneous distributions of their resulting plumes—influences particle aging and associated properties including CCN activity. Present aerosol-aware models at regional and global scales possess insufficient resolution to capture the full spatial heterogeneity of aerosols and the emissions of primary aerosols and gas phase precursors. In turn, these models depict artificially dilute and uniform concentrations within grid cells. This alters the representation of concentration-dependent, non-linear aerosol processes such as coagulation and gas particle partitioning. Past studies have shown that climate-relevant aerosol properties such as aerosol optical properties (Gustafson Jr. et al., 2011) and CCN activity (Weigum et al., 2016) are highly sensitive to the model's grid resolution with a large contribution of sub-grid scale variability resulting from the spatially varying pattern of emissions (Qian et al., 2010).

Past studies evaluating the sub-grid variability of aerosol properties often compare outputs from models with coarse resolution typical of global climate models (~ 50–100 km) against higher resolution model outputs with resolution on the order of ~ 1–10 km (Qian et al., 2010; Gustafson Jr. et al., 2011; Weigum et al., 2016; Crippa et al., 2017; Lin et al., 2017). While such improvements in resolution better resolve heterogeneities in emissions, there still exists considerable unresolved spatial heterogeneity in the sub-kilometer scale. In addition, such modeling studies do not explicitly resolve the scales of turbulent transport in the boundary layer, instead fully parameterizing turbulence via Reynolds-averaged Navier Stokes.

The evolution of emission plumes containing gas phase compounds and aerosols is highly dependent on turbulent mixing at fine spatial scales and the proximity of reactive species. A considerable body of literature has investigated the role of turbulence-chemistry interactions and chemical segregation on gas phase reactions in the planetary boundary layer via the use of large-eddy simulations (LES). Brasseur et al. (2023) review recent applications of LES to investigate chemical segregation and turbulence chemistry interactions in a variety of spatially heterogeneous geographic regions. Past studies tend to focus on the oxidation of highly reactive volatile organic compounds (VOCs) such as isoprene and have shown that spatially heterogeneous emissions contribute to the chemical segregation between reactive gas phase species in the boundary layer (Ouwersloot et al., 2011; Kaser et al., 2015). Note, however, that these studies do not model aerosols, although the coupling between the gas phase and aerosols through gas-particle partitioning suggests chemical segregation due to the spatial heterogeneity of emissions likely influences the aerosol state.

Recently, numerous turbulence-resolving frameworks have been coupled to aerosol models including the use of the Sectional Aerosol model for Large Scale Applications (SALSA) (Kokkola et al., 2008) alongside UCLALES (Tonttila et al., 2017) and the Parallelized Large-Eddy Simulation Model (PALM) (Kurppa et al., 2019) as well as the coupling between the modal model M7 (Vignati et al., 2004) and the Dutch Atmospheric Large-Eddy Simulation model (DALES) (de Bruine et al., 2019). Although these models have high-resolution transport schemes, they each possess relatively coarse-resolution aerosol treatments. For instance, UCLALES-SALSA uses a 10-bin sectional treatment while DALES implements a modified version of the seven-mode M7 model to allow two additional hydrometeor modes. To our knowledge, no aerosol-aware transport model has yet to leverage a high-resolution particle resolved aerosol treatment alongside turbulence resolving transport frameworks such as LES.

Past research has established a clear link between the spatial heterogeneity of both gas phase and aerosol emissions, the processes by which the aerosol age, and their resulting climate-relevant properties including CCN activity which contribute to indirect radiative forcing. Simultaneously, there exists large uncertainty in the radiative forcing due to aerosols which results in part from the coarse representation of both aerosols and their transport in global scale models and their coupling with non-linear processes that occur at the sub-grid scale such as coagulation and turbulence-chemistry interactions. Past research has led to the development of detailed aerosol model treatments and transport representations, however there has yet to be a direct coupling between particle-resolved aerosol models and turbulence-resolving transport models for use in quantifying the effects of emissions spatial heterogeneity on the aerosol state and CCN activity.

The aim of this work is to conduct a process-level analysis of the the complex coupling between the spatial heterogeneity of surface emissions (including both gas compounds and primary aerosol), aerosol aging processes, and the resulting impact on aerosol properties including CCN activity via a set of first-of-a-kind particle-resolved LES. This establishes a high resolution aerosol-transport model framework in both explicit representation of turbulent transport as well as aerosol composition, properties, and aging.

This paper is organized in the following manner. Section 2 presents the modeling framework used in this study, WRF-PartMC-MOSAIC-LES, alongside a description of numerous emissions scenarios ranging in spatial heterogeneity. Section 3 discusses results of simulation runs, and a description of changes to the aerosol size distribution, composition, hygroscopicity,

and CCN activity across emissions scenarios are discussed. We conclude with remarks on the implications of this study, limitations stemming from its idealized nature, and future work.

2   Methods

2.1   WRF-PartMC-MOSAIC-LES

The aerosol-transport model WRF-PartMC-MOSAIC-LES is a coupling of numerous sub-models responsible for transport, the aerosol representation, and multiphase chemistry. WRF-PartMC-MOSAIC-LES is an extension of the aerosol-transport model WRF-PartMC, which was developed by (Curtis et al., 2017) for particle diffusion and recently extended to include advection (Curtis et al., 2024). WRF-PartMC couples the Weather Research and Forecasting model (WRF) (Skamarock et al., 2008) and the particle-resolved aerosol model Particle Monte Carlo (PartMC) (Riemer et al., 2009). PartMC represents a population of aerosol particles using an ensemble of computational particles, each with appropriate weighting (i.e., particle multiplicity) to represent the diversity of particle sizes and composition apparent in actual aerosol populations. The composition of each computational particle is allowed to vary as particles age. PartMC is a box model, meaning that the relative position of particles within computational grid cells is not tracked. Instead, the transport of particles into and out of grid cells is handled by a stochastic advection algorithm housed in the interface between PartMC and the dynamical model WRF (Curtis et al., 2024). WRF-PartMC has been used in a 1-dimensional setting to resolve vertical gradients in aerosol composition and mixing state (Curtis et al., 2017) and more recently in a 3-dimensional setting to illustrate transport of particles by simulated meteorology over a regional domain (Curtis et al., 2024).

LES models explicitly resolve large scales of turbulent motion; however, they must parameterize eddies which cannot be resolved below the grid resolution on the order of 10–100 m and the down-gradient tendency of turbulent kinetic energy (TKE) to be transferred from large to small scales, ultimately dissipating as heat energy. This requires use of eddy diffusivity and eddy viscosity parameterizations, and WRF-PartMC-MOSAIC-LES utilizes Deardorff's TKE scheme (Deardorff, 1980).

Both gas-phase and aerosol chemistry are represented using the Model for Simulating Aerosol Interactions and Chemistry (MOSAIC) (Zaveri et al., 2008). MOSAIC is comprised of numerous sub-models, including the Carbon Bond Mechanism version Z (CBM-Z) which solves gas phase chemistry (Zaveri and Peters, 1999). Phase-dependent partitioning of aerosol species is handled by the Multicomponent Equilibrium Solver for Aerosols (MESA) (Zaveri et al., 2005a). Activity coefficients of electrolytes are parameterized via the multicomponent Taylor expansion method (MTEM) (Zaveri et al., 2005b). In order to solve the numerically stiff set of solid-liquid phase reactions governing thermodynamic equilibrium, MOSAIC utilizes the adaptive step time-split Euler method (ASTEM) (Zaveri et al., 2008). MOSAIC models aerosol chemistry for both inorganic and organic compounds such as nitrate, ammonium, sulfate, black carbon (BC), and a limited set of secondary organic aerosol (SOA) species.

2.2 Computational domain setup

The computational domain has a horizontal extent of 10 km in both x- and y-axes, with horizontal grid spacing of 100 m. In the vertical, the domain extends to 2 km and is represented with 200 vertical levels. WRF uses an η vertical coordinate system and for LES runs, vertical levels are linearly spaced in pressure. This results in an effective vertical grid spacing of approximately 10 m. Simulations are configured to begin on the Vernal Equinox at 09:00 local time and conclude at 15:00 for a total duration of 6 hours in order to balance photolysis rates throughout simulations. Each grid cell is initialized with 100 computational particles, resulting in 100 million total particles.

The surface of the domain is characterized by a uniform, flat surface absent of topographical features or land-use variations. Note that WRF-PartMC-MOSAIC-LES is not coupled to one of WRF's radiation sub-models. Instead, MOSAIC utilizes idealized parameterizations to determine photolysis rates based on the solar zenith angle. Due to the lack of a radiation sub-model, surface heating is imposed uniformly across the domain using a constant rate of 0.24 K m^{-1} s^{-1}.

Both aerosol and gas phase initial conditions and emissions are chosen to represent species and concentrations typical of an urban plume and are adopted from Riemer et al. (2009). Initial concentrations and emission rates were adapted from the 1987 Southern California Air Quality Study (SCAQS) during which measurements of gas phase species and particulate matter mass concentrations were collected at multiple sites across the Los Angeles basin (Zaveri et al., 2008). Table 1 contains initial concentrations and emission rates for gas phase species. Table 2 includes aerosol initial conditions and emission rates organized by aerosol modes. Initially, the aerosol is an equal mixture of ammonium sulfate and primary organic aerosol (POA). The three emission modes including cooking and vehicular combustion are varied mixtures of POA and BC. To allow for simulation spin-up during which time the convective boundary layer fully develops, all emission rates are set to zero during the first hour of simulations. Subsequently, emitted compounds are released at the surface at constant rates indicated by Tables 1 and 2 for the remainder of simulations.

Meteorological initial conditions are specified using an idealized sounding for a convective boundary layer where the surface is 5 K warmer than the mixing layer and is capped by an inversion of 8 K at 1 km. The wind profile is zero throughout the entire vertical extent of the domain.

2.3 Emissions Scenarios

We evaluate the impacts of emissions spatial heterogeneity on aerosol properties via numerous emissions scenarios shown in Figure 1. Emissions are first released uniformly over the entire domain. This scenario, referred to as the uniform base case, serves as a proxy for coarser resolution models which do not resolve the spatial heterogeneity of emissions and instead emit gas compounds and primary aerosol in a uniform and diffuse manner across grid cells. Successive scenarios are compared against this uniform base case to evaluate modifications to aerosol properties resulting from the spatial heterogeneity of emissions. Scenario 1 represents an idealized depiction of an urban-rural interface, whereby emissions are released in half the domain with no emissions occurring in the other half. Scenario 2 contains a narrow strip of emissions running through the center of the

5

Table 1. Gas phase emissions and initial conditions. Table adapted from Riemer et al. (2009) with permission.

Species	Symbol	Initial Mole Fraction (ppb)	Emissions (nmol m^{-2} s^{-1})
Nitric oxide	NO	0.1	31.8
Nitrogen dioxide	NO$_2$	1.0	1.67
Nitric acid	HNO$_3$	1.0	
Ozone	O$_3$	50.0	
Hydrogen peroxide	H$_2$O$_2$	1.1	
Carbon monoxide	CO	21	291.3
Sulfur dioxide	SO$_2$	0.8	2.51
Ammonia	NH$_3$	0.5	6.11
Hydrogen chloride	HCl	0.7	
Methane	CH$_4$	2200	
Ethane	C$_2$H$_6$	1.0	
Formaldehyde	HCHO	1.2	1.68
Methanol	CH$_3$OH	0.12	0.28
Methyl hydrogen peroxide	CH$_3$OOH	0.5	
Acetaldehyde	ALD2	1.0	0.68
Paraffin carbon	PAR	2.0	96
Acetone	AONE	1.0	1.23
Ethene	ETH	0.2	7.2
Terminal olefin carbons	OLET	$2.3 \cdot 10^{-2}$	2.42
Internal olefin carbons	OLEI	$3.1 \cdot 10^{-4}$	2.42
Toluene	TOL	0.1	4.04
Xylene	XYL	0.1	2.41
Lumped organic nitrate	ONIT	0.1	
Peroxyacetyl nitrate	PAN	0.8	
Higher organic acid	RCOOH	0.2	
Higher organic peroxide	ROOH	$2.5 \cdot 10^{-2}$	
Isoprene	ISOP	0.5	0.23
Alcohols	ANOL		3.45

155 domain, corresponding to an emission pattern typical of a busy roadway. Lastly, scenario 3 places all emissions in a single grid cell in the center of the domain and is representative of a point-source emission, such as a plume from an industrial source.

Table 2. Aerosol emissions and initial conditions. Table adapted from Riemer et al. (2009) with permission.

Initial/Background	N (m^{-3})	D_{gn} (μm)	σ_g	Composition by Mass
Aitken Mode	$3.2 \cdot 10^9$	0.02	1.45	50% (NH$_4$)$_2$SO$_4$, 50% POA
Accumulation Mode	$2.9 \cdot 10^9$	0.116	1.65	50% (NH$_4$)$_2$SO$_4$, 50% POA

Emissions	E (m^{-2} s^{-1})	D_{gn} (μm)	σ_g	Composition by Mass
Meat cooking	$9 \cdot 10^6$	0.086	1.9	100% POA
Diesel vehicles	$1.6 \cdot 10^8$	0.05	1.7	30% POA, 70% BC
Gasoline vehicles	$5 \cdot 10^7$	0.05	1.7	80% POA, 20% BC
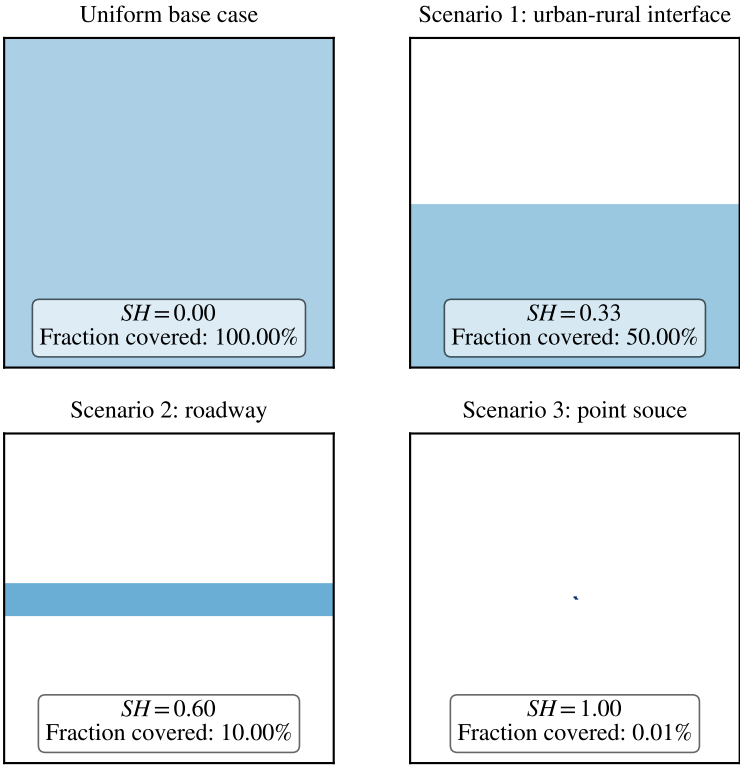
Figure 1.

Emissions scenarios are chosen to represent a range of spatial heterogeneity, which is quantified using the SH metric of (Mohebalhojeh et al., 2024) make sure to update this citation when Matin's paper is published. The SH metric is a normalized

measure of spatial heterogeneity, ranging from 0 (fully homogeneous) to 1 (fully heterogeneous). Thus, the uniform base case corresponds to the homogeneous condition while scenario 3—point source emission—represents the maximally heterogeneous emissions scenario. To ensure the mass of gas species and aerosol emitted per unit of time is consistent across each scenario, emission rates are divided by the fraction of area covered by emissions. For instance, in scenario 3, this results in a scaling of $10,000$ for the point-source emission. The fraction of area covered by emissions is displayed for each scenario alongside the spatial heterogeneity as quantified via the metric of Mohebalhojeh et al. (2024) in Figure 1.

3 Results

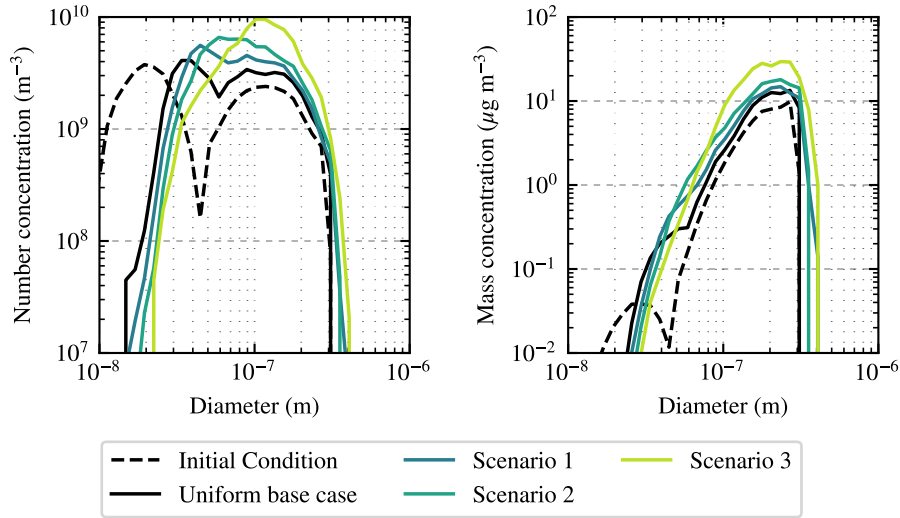### 3.1 Aerosol size distributions

Figure 2.

Number and mass distributions for each emissions scenario are shown in Figure 2. The initial condition is corresponds to the black dashed line, indicating a bimodal distribution of Aitken and accumulation mode particles. Solid lines indicate the distribution at the end of each simulation ($t = 6$ h). The uniform base case corresponds to the solid black line, where emissions scenarios are indicated by colored solid lines. Each size distribution is taken from a vertical level in the upper boundary layer at $z \approx 800$ m. Due to the stochastic treatment of aerosol particles in WRF-PartMC and the selected number of computational particles per grid cell ($N = 100$), both number and mass distributions represent the average distribution in a 1 km^2 region centered over the emissions plume (i.e., size distributions are averaged over a 10×10 grid cell region). For the uniform base case, scenario 2 and scenario 3, this region is directly over the center of the domain. For scenario 1, emissions are released in

175 one half of the domain that is offset from the center, and thus the averaging region is located in the center of the emissions patch. For each size distribution, data have been binned into 100 bins, ranging in size from 10^{-9} to 10^{-3} m.

As the spatial heterogeneity of emissions increases from the uniform base case to scenario 3, we find that the number of Aitken mode particles decreases while the number of accumulation mode particles increases. This points to enhanced Brownian coagulation among ultra-fine particles as a result of higher local concentrations near the emissions plume core.

180 For scenarios with high emissions spatial heterogeneity, the mass distribution in the accumulation mode increases while a slight decrease is observed in the Aitken mode. Coagulation of smaller Aitken mode particles with accumulation mode particles contributes little change in the mass distribution as indicated by a slight reduction in the Aitken mode mass concentration. This indicates that the increase in mass concentration in the accumulation mode is largely due to gas-particle partitioning, which will be discussed in detail in the next section.
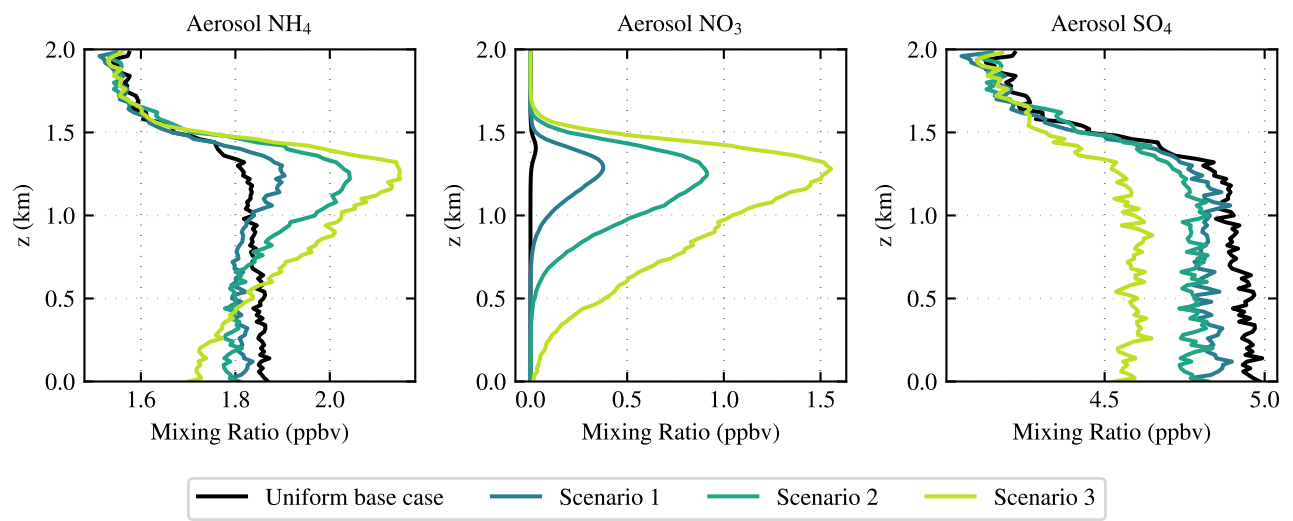
185 3.2 Aerosol composition

Figure 3. Modify the linewidth, a bit too thick

Figure 3 shows vertical profiles of aerosol ammonium (NH_4), nitrate (NO_3), and sulfate (SO_4) for each emissions scenario. The uniform base case is indicated via the solid black line while scenarios are indicated by colored lines ranging from blue (low spatial heterogeneity) to light green (high spatial heterogeneity). These profiles represent the average concentration of aerosol species within each vertical level at the end of each simulation ($t = 6$ h).

190 Sulfate concentrations are nearly uniform within the boundary layer and rapidly decrease above the entrainment zone due to little exchange between the free troposphere and the boundary layer. Sulfate concentrations decrease as the emissions spatial heterogeneity is increased. Note that for scenarios with high emissions spatial heterogeneity, the elevated concentration of reactive gas phase compounds in the emissions plume such as volatile organic compounds (VOCs) alongside sulfate's gas

phase precursor SO_2 results in greater effective competition for oxidation with OH. As a result, OH is rapidly depleted near the emissions plume, thereby reducing the potential for oxidation of SO_2 to form H_2SO_4 (which rapidly partitions into the aerosol phase as sulfate owing to its extremely low volatility vapor pressure). OH from outside the emissions plume is not mixed and entrained into the plume fast enough to restore its concentration, thereby illustrating the impact of emissions spatial heterogeneity in chemically segregating reactive gas phase species OH and SO_2, and in altering the subsequent formation of sulfate through gas-particle partitioning.

Both ammonium and nitrate concentrations increase with height in the boundary layer due to the strong temperature dependence of ammonium nitrate formation. The abundance of nitrate depends on the availability of free ammonia, that is, ammonia in excess of what is required to neutralize sulfate as ammonium sulfate. In the lowest 500 m of the boundary layer, the concentration of NH_4 decreases as the emissions spatial heterogeneity increases. What might be the physical reasoning for this? Perhaps the lower concentration of sulfate in high SH scenarios drives the equilibrium condition to the gas phase? Note that when the particles are sulfate rich, they are highly acidic and thus allow absorption of any available NH3 so perhaps the reverse is occurring in this case? As emissions spatial heterogeneity increases, greater NH_4 and NO_3 form as ammonium nitrate in the aerosol phase towards the top of the boundary layer ($z \sim 1.2$ km at $t = 6$ h). The decrease in sulfate concentrations for scenarios with high emissions spatial heterogeneity results in higher concentrations of free ammonia, thus allowing the formation of more ammonium nitrate. Note that in the uniform base case, almost no nitrate is formed due to the lack of free ammonium as nearly all NH_4 is bound to sulfate as ammonium sulfate. This indicates the strong dependence of nitrate concentrations on the composition of the aerosol and the level of emissions spatial heterogeneity.

Figure 4 shows the size-resolved mass fraction of aerosols in the upper boundary layer ($z \approx 800$ m) for the initial condition and at the end of simulations ($t = 6$ h) for both the uniform base case and the maximally spatially heterogeneous emissions scenario, scenario 3. After 6 hours, a stark difference in composition is apparent between particles in the uniform base case and scenario 3. Under uniform, dilute emissions, particles are largely comprised of BC and organic carbon (OC) along with some sulfate. Particles that age under the spatially heterogeneous emissions of scenario 3 are dominated by nitrate, ammonium, and sulfate and jointly comprise between 50 to 80% of aerosol mass.

The CCN activity of particles in the size range of 50-100 nm is largely dependent on their composition—in the presence of hygroscopic aerosol, the solute effect of Raoult's Law lowers the critical supersaturation required for activation. Without the aid of hygroscopic material, small aerosol particles possess high critical supersaturations due to the Kelvin effect which increases vapor pressure over the particle surface due to its curvature. Figure 4 indicates that, for the uniform base case, particles in the size range of 50-100 nm are primarily composed of BC and OC (low hygroscopicity compounds) whereas sulfate, nitrate, and ammonium dominate the mass fraction in the same size range for the high emissions spatial heterogeneity scenario. This indicates that particles in the size range whose CCN activity hinges on aerosol composition are more hygroscopic under high emissions spatial heterogeneity scenarios and thus activate at lower supersaturations.

Figure 5 shows 2-dimensional number distributions $n(D_p, \kappa)$ as a function of particle diameter D_p and particle hygroscopicity parameter κ in the upper boundary layer ($z \approx 800$ m). Particles are binned into a two-dimensional histogram by diameter (50 bins ranging from 10 nm to 1 μm) and bins are colored by their corresponding number concentration indicated by the
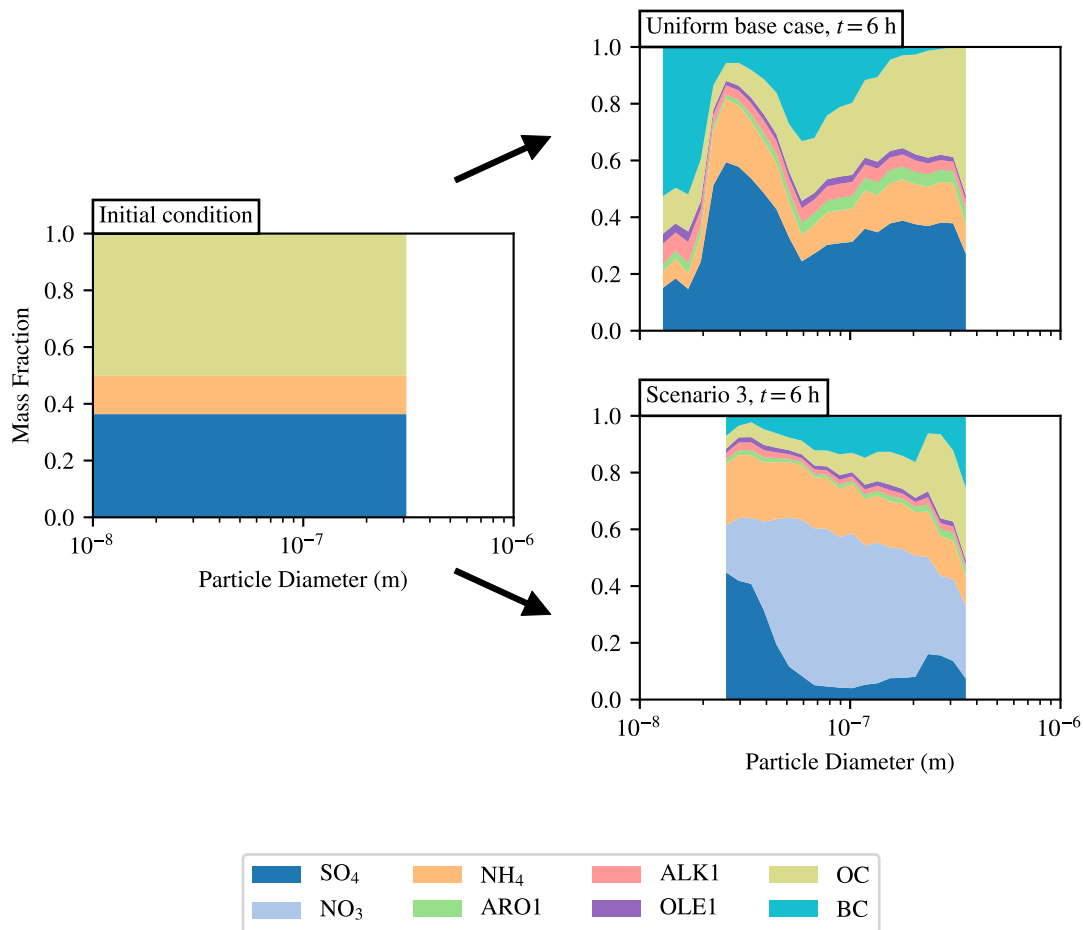
Figure 4. Size-resolved mass fraction for emissions scenario 3 at regular 2-hour intervals showing species mass fraction as a percent of total aerosol mass vs. particle diameter.

colorbar. The initial condition is shown on the left whereby all particles possess the same composition and thus the same hygroscopicity. The inclusion of ammonium sulfate in the initial condition makes the particles moderately hygroscopic. On the right, the 2-dimensional size distribution is shown at the end of simulations ($t = 6$ h) for both the uniform base case and the maximally spatially heterogeneous scenario, scenario 3.

Two primary groupings of particles are noticeable for the uniform base case—a grouping of lower κ particles between $\kappa = 0$ and $\kappa \approx 0.3$ alongside a grouping of particles with higher κ ranging from $\kappa \approx 0.3$ to $\kappa \approx 0.6$. The grouping of lower κ particles correspond to carbonacous primary aerosol which have not undergone significant aging in the form of coagulation and gas-particle partitioning which increase the fraction of hygroscopic compounds (such as sulfate, nitrate, and ammonium). The
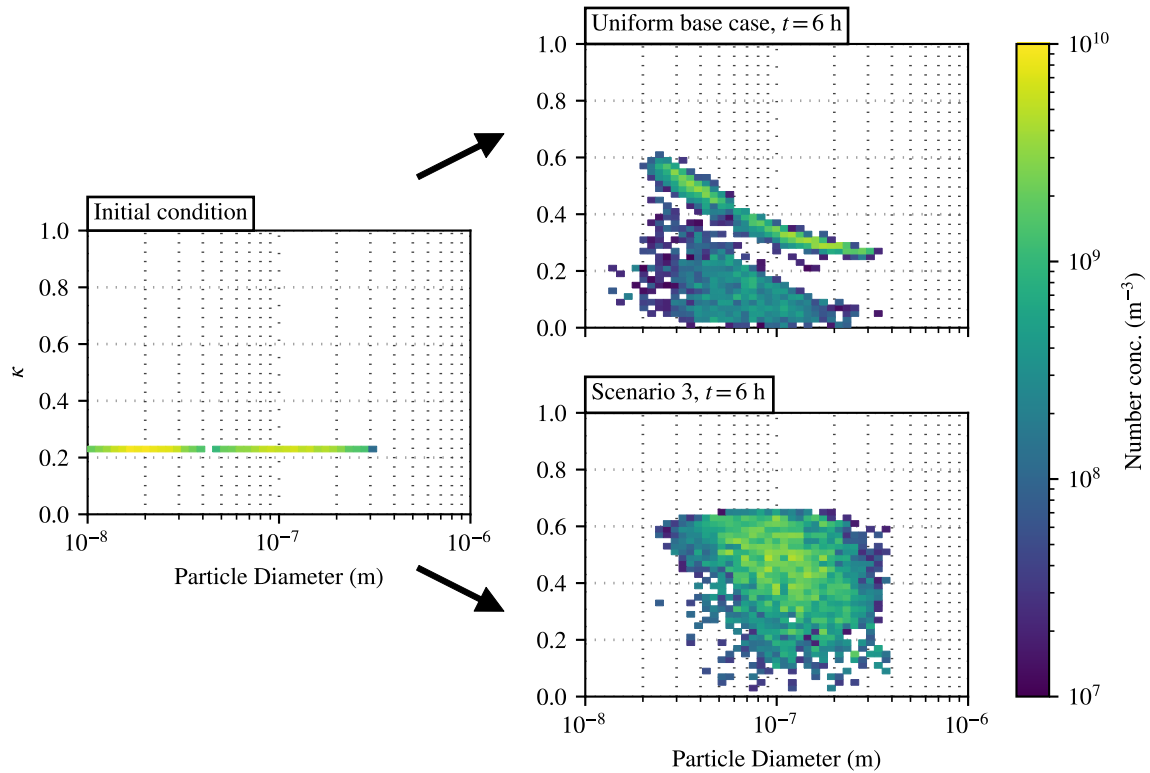
11

Figure 5. 2-dimensional number distributions $n(D_p, \kappa)$ at regular two-hour intervals for scenario 3.

upper band of higher κ particles is shown to increase towards smaller particles, consistent with the elevated levels of sulfate observed in particles between 20–50 nm in the uniform base case shown in Figure 4.

By comparison to the uniform base case, the number distribution for scenario 3 indicates the presence of higher κ particles. For instance, the hygroscopicity of particles with diameter of 100 nm is in excess of $\kappa > 0.6$ for scenario 3 (indicating highly hygroscopic particles), whereas κ only reaches up to 0.4 for 100 nm particles in the uniform base case. These findings show that spatially heterogeneous emissions can elevate the hygroscopicity of particles whose CCN activity is dependent on particle composition ($D_p \sim 50$–100 nm).

Note that differences in the 2-dimensional number distributions with regard to κ between the uniform base case and scenario 3 can be attributed to the coupling between emissions spatial heterogeneity and sub-grid scale aerosol processes. As previously noted, the enhancement of coagulation in spatially heterogeneous emission plumes reduces the concentration of Aitken mode particles. This helps explain the absence of a grouping of low-κ carbonaceous primary aerosol particles. Furthermore, enhancements to gas-particle partitioning due to spatially heterogeneous emissions are responsible for increasing the hygroscopicity of particles. In particular, the formation of ammonium nitrate in scenario 3 due to reduced levels of sulfate and a corresponding increase in free ammonia elevate particle hygroscopicity.
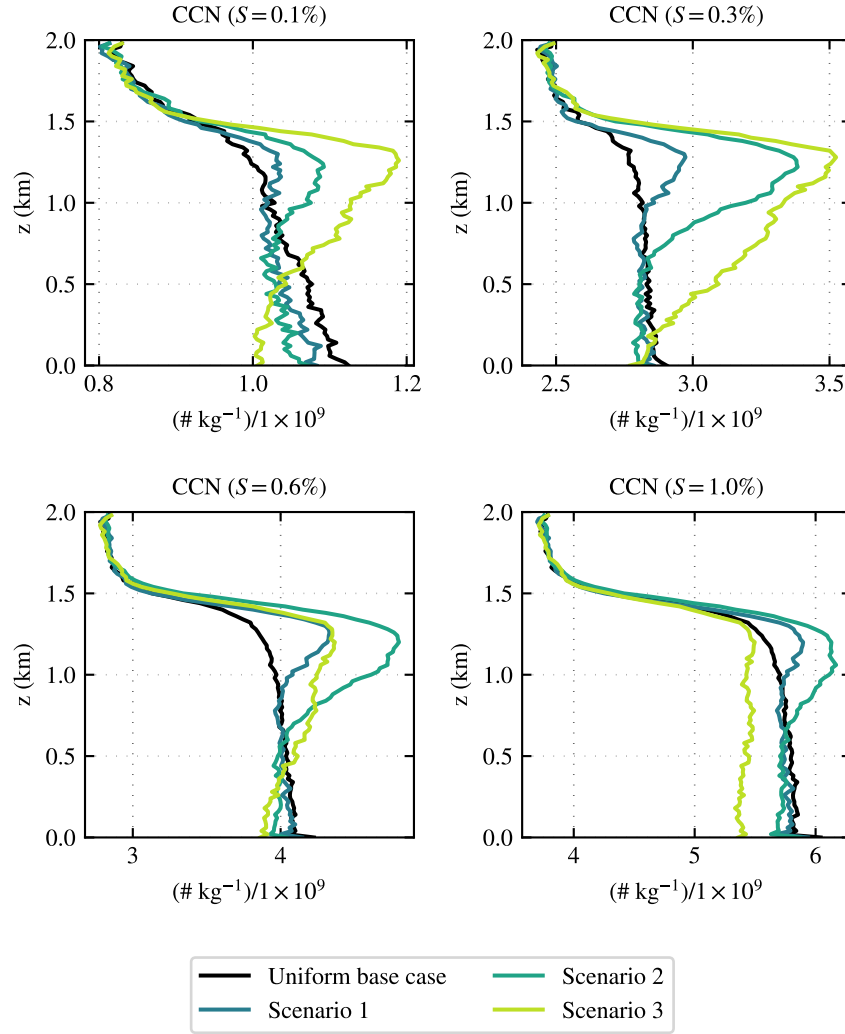
3.3 CCN activity

Figure 6.

Figure 6 shows vertical profiles of the CCN number concentration per kilogram of dry air for supersaturations S ranging from $S = 0.1\%$ to $S = 1.0\%$ and for each emissions scenario. Note that the ambient relative humidity (RH) in each simulation does not exceed 100%—instead, reported CCN concentrations indicate the number of particles that would activate given the RH were raised to the specified supersaturation.

As noted previously, the coupling between emissions spatial heterogeneity and aerosol processes such as coagulation and gas-particle partitioning are responsible for altering the number, size, composition, and hygroscopicity of particles. These

processes in turn modify the resulting CCN activity; however, the dominant processes contributing to changes in CCN activity and the strength of effect vary with supersaturation.

At low supersaturations ($S = 0.1$–0.3%), CCN activity increases with emissions spatial heterogeneity in the upper boundary layer due to enhanced formation of ammonium nitrate in the cooler, sulfate poor environment. This elevates activation of ultrafine particles in the range of 50–100 nm due to the high hygroscopicity of ammonium nitrate.

At higher supersaturations ($S = 0.6$–1.0%), an increase in CCN activity in the upper boundary layer is still found for emissions scenarios with lower spatial heterogeneity, however, at high emissions heterogeneity (scenario 3), the number concentration is reduced. This effect is most prominent at the highest supersaturation ($S = 1.0\%$), whereby the number concentration of CCN throughout the boundary layer is less than all other scenarios including the uniform base case. This phenomenon is due to the enhancement of coagulation by the emissions spatial heterogeneity and illustrates how coagulation has a competing effect on CCN activity which dominates at high supersaturations. Note that small, non-hygroscopic particles possess high critical supersaturations. Additionally, the enhancement to coagulation for emissions scenarios with high spatial heterogeneity acts to efficiently remove smaller particles. Therefore, at sufficiently high supersaturation and emissions spatial heterogeneity, the negative effect on CCN activity due to coagulation will dominate the positive effect introduced by gas-particle partitioning of hygroscopic material.

Figure 7 shows time vs. height plots of the percent difference between the CCN concentrations at each supersaturation level and emissions scenario and the corresponding CCN concentrations in the uniform base case. Percent difference is calculated as

$$\% \text{ difference} = 100 \times \left(\frac{\overline{[\text{CCN}]}(t,z,S)_{\text{Scenario}} - \overline{[\text{CCN}]}(t,z,S)_{\text{Base case}}}{\overline{[\text{CCN}]}(t,z,S)_{\text{Base case}}} \right), \tag{1}$$

where $\overline{[\text{CCN}]}(t,z,S)_{\text{Scenario}}$ is the horizontally averaged concentration of CCN at time t and vertical level z that activate at supersaturation S for the given emissions scenario and $\overline{[\text{CCN}]}(t,z,S)_{\text{Base case}}$ is the horizontally averaged concentration of CCN at time t and vertical level z that activate at supersaturation S for the uniform base case.

The greatest increase in CCN activity occurs for scenario 3, the highest spatial heterogeneity emissions scenario, at a supersaturation of $S = 0.3\%$ whereby CCN concentrations increase by upwards of 25% through $t = 6$ h. Across each scenario, the location of greatest increase in CCN activity grows with time due to boundary layer development. Moving down (higher supersaturation) and to the right (higher emissions spatial heterogeneity) in Figure 7, the reduction in CCN activity due to the enhancement of coagulation (see discussion of Figure 6 for a process-level description) manifests after approximately 5 hours of simulation. Anything else to say about this figure?

3.4 Influence of ammonia on aerosol composition and CCN activity

We have shown that CCN activity is modulated by emissions spatial heterogeneity due to enhancements to coagulation and the gas-particle partitioning of ammonia and nitric acid to form ammonium nitrate which elevates particle hygroscopicity. Furthermore, the formation of ammonium nitrate is governed by the availability of free ammonia. To investigate the sensitivity of changes in CCN activity due to the presence of ammonia in spatially heterogeneous emissions, a set of two additional simula-
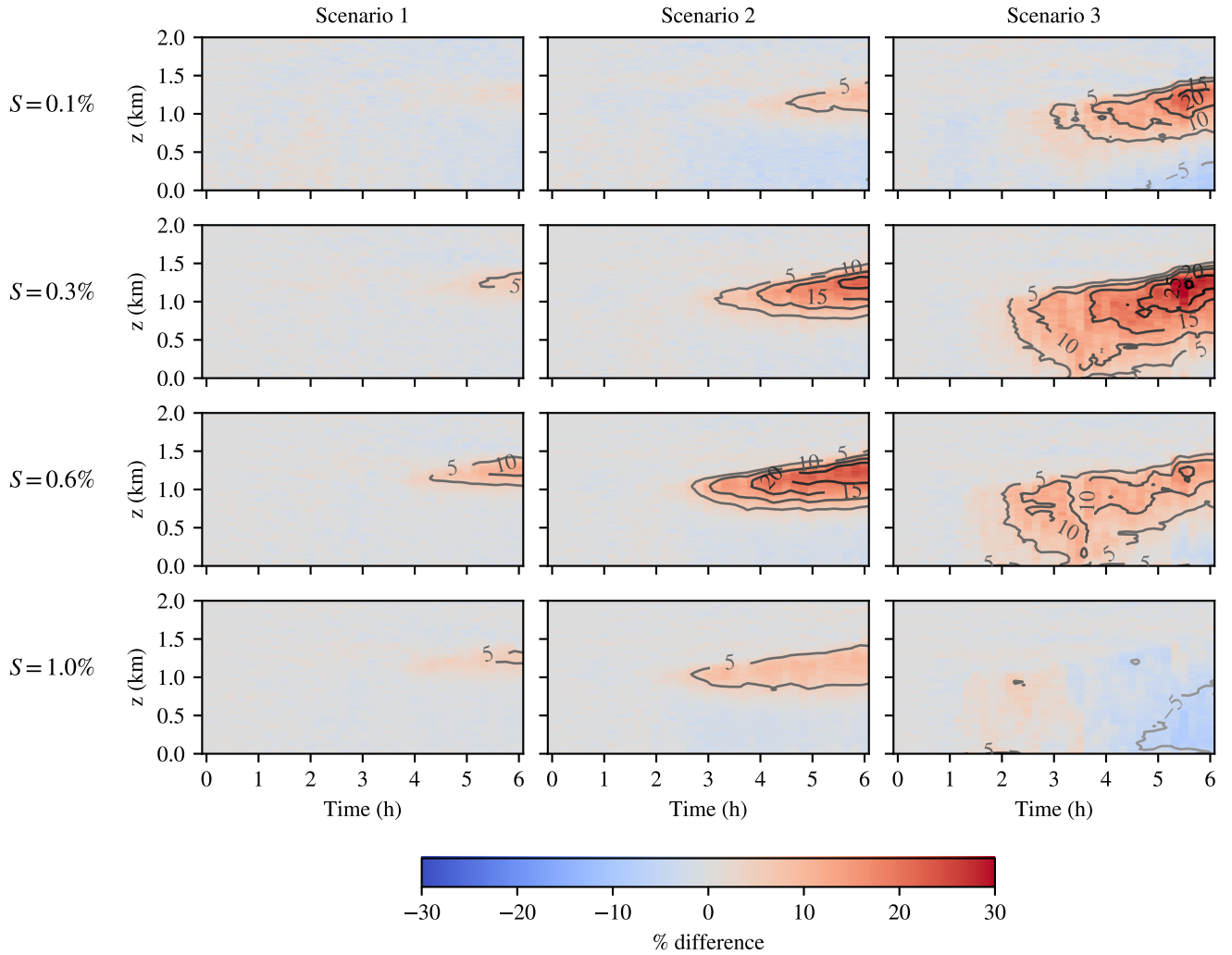
14

Figure 7.

tions were run for the uniform base case and scenario 3 in which the concentration of total ammonium ($NH_{3, \text{gas}} + NH_{4, \text{aerosol}}$) is set to zero. Emissions of NH_3 are also set to zero to ensure that total ammonium remains zero throughout each simulation.

Figure 8 shows vertical profiles of CCN concentrations in number of particles per kilogram of dry air at supersaturations ranging from $S = 0.1\%$ to $S = 1.0\%$ and at $t = 6$ h. Profiles for simulations containing ammonia are displayed as solid lines while simulations without ammonia are shown as dashed lines. We find that, without ammonia, CCN concentrations at each supersaturation level agree much closer. The peak of CCN concentrations in the upper boundary layer and at lower supersaturations found for scenario 3 with ammonia is entirely absent. This underscores the significance of the coupling between spatially
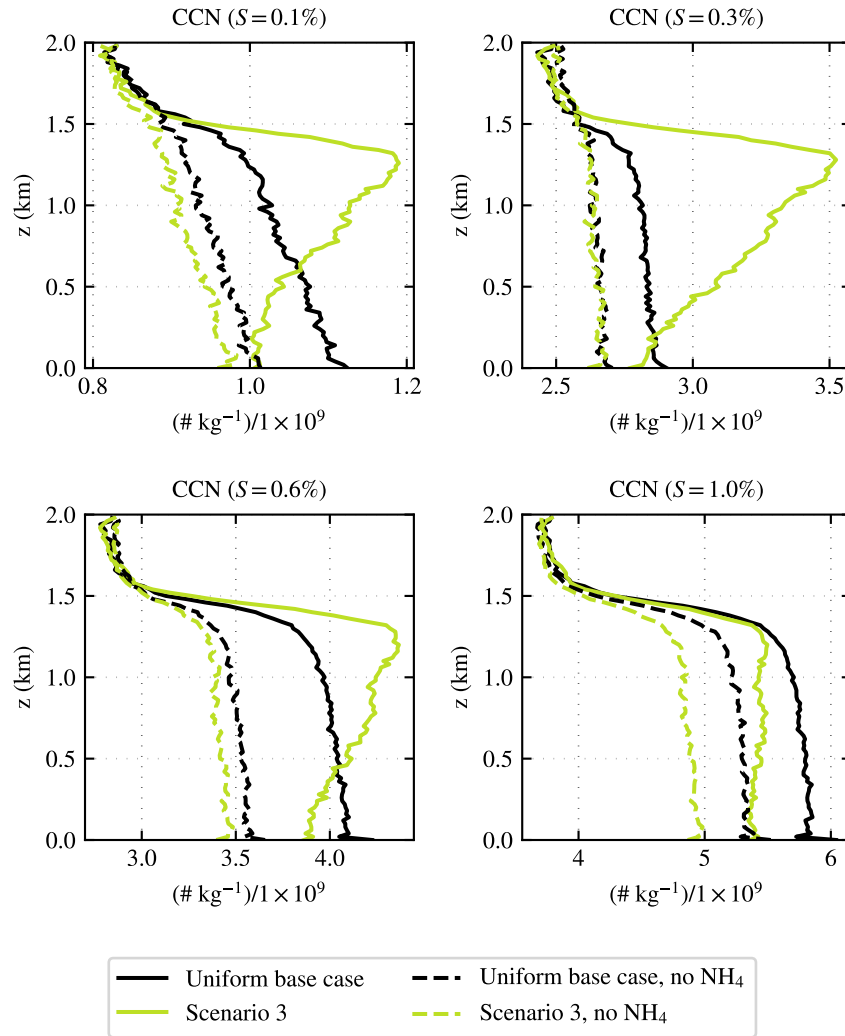
Figure 8.

heterogeneous emissions, their composition, and the formation of ammonium nitrate via gas-particle partitioning in altering CCN activity, especially at lower supersaturations.

300   At higher supersaturations, particularly at $S = 1.0\%$, the reduction in CCN concentrations for scenario 3 without ammonia relative to the corresponding uniform base case point to the enhancement of coagulation under spatially heterogeneous emissions. Without the countervailing effect of gas-particle partitioning in increasing CCN activity due to ammonium nitrate formation, the vertical profiles of the ammonia-free uniform base case and scenario 3 closely match each other, albeit with an offset for scenario 3 due to the enhancement of coagulation that shifts the number concentration lower by approximately 5%.

16

4 Conclusions

This study investigates the impacts of spatially heterogeneous emissions on aerosol properties in a convective boundary layer including CCN activity using a first-of-a-kind particle-resolved large-eddy simulation modeling framework, WRF-PartMC-MOSAIC-LES. This platform permits a process level analysis of the coupling between emissions spatial heterogeneity and concentration dependent aerosol processes such as coagulation and gas-particle partitioning. Emissions spatial heterogeneity is varied using numerous idealized scenarios and are compared against a base case of uniform emissions which acts as a proxy for coarser-resolved models whose grid resolution is insufficient to represent the underlying spatial heterogeneity of emissions.

Key aerosol processes including gas-particle partitioning and coagulation are impacted by emissions spatial heterogeneity, as we find significant changes to the sulfate-nitrate-ammonium system and an increased rate of coagulation under high emissions spatial heterogeneity scenarios.

Changes to aerosol processes have downstream effects on CCN activity. Furthermore, modifications by emissions spatial heterogeneity to coagulation and gas-particle partitioning result in competing effects on the concentration of CCN at a given supersaturation level. Coagulation removes smaller particles that activate at high supersaturations, resulting in a decrease in CCN activity at high supersaturations for scenarios with high emissions spatial heterogeneity. Conversely, coagulation is not as efficient at removing larger particles that activate at lower supersaturations and gas-particle partitioning results in an increase of highly hygroscopic compounds such as ammonium nitrate under high emissions spatial heterogeneity. As a result, CCN activity at lower supersaturations ($S = 0.3$—0.6%) increases by up to 25% in the upper boundary layer for emissions scenarios with high spatial heterogeneity.

The effect of emissions spatial heterogeneity on CCN activity is highly dependent on the composition of the aerosol and gas phase. Given the key contribution of ammonium nitrate formation in elevating CCN activity under highly spatially heterogeneous scenarios, the removal of ammonia decreases—or in some cases reverses—the trend between emissions spatial heterogeneity and CCN activity.

Code availability. TEXT

Data availability. TEXT

Code and data availability. TEXT

Sample availability. TEXT

17

Video supplement. TEXT

Appendix A

A1

Author contributions. TEXT

335 *Competing interests.* TEXT

Disclaimer. TEXT

Acknowledgements. TEXT

References

Brasseur, G. P., Barth, M., Kazil, J., Patton, E., and Wang, Y.: Segregation of Fast-Reactive Species in Atmospheric Turbulent Flow, https://doi.org/10.20944/preprints202305.0895.v1, 2023.

Ching, J., Fast, J., West, M., and Riemer, N.: Metrics to quantify the importance of mixing state for CCN activity, Atmospheric Chemistry and Physics, 17, 7445–7458, https://doi.org/10.5194/acp-17-7445-2017, publisher: Copernicus GmbH, 2017.

Crippa, P., Sullivan, R. C., Thota, A., and Pryor, S. C.: The impact of resolution on meteorological, chemical and aerosol properties in regional simulations with WRF-Chem, Atmospheric Chemistry and Physics, 17, 1511–1528, https://doi.org/10.5194/acp-17-1511-2017, publisher: Copernicus GmbH, 2017.

Curtis, J. H., Riemer, N., and West, M.: A single-column particle-resolved model for simulating the vertical distribution of aerosol mixing state: WRF-PartMC-MOSAIC-SCM v1.0, Geoscientific Model Development, 10, 4057–4079, https://doi.org/10.5194/gmd-10-4057-2017, publisher: Copernicus GmbH, 2017.

Curtis, J. H., Riemer, N., and West, M.: Explicit stochastic advection algorithms for the regional-scale particle-resolved atmospheric aerosol model WRF-PartMC (v1.0), Geoscientific Model Development, 17, 8399–8420, https://doi.org/10.5194/gmd-17-8399-2024, 2024.

de Bruine, M., Krol, M., Vilà-Guerau de Arellano, J., and Röckmann, T.: Explicit aerosol–cloud interactions in the Dutch Atmospheric Large-Eddy Simulation model DALES4.1-M7, Geoscientific Model Development, 12, 5177–5196, https://doi.org/10.5194/gmd-12-5177-2019, publisher: Copernicus GmbH, 2019.

Deardorff, J. W.: Stratocumulus-capped mixed layers derived from a three-dimensional model, Boundary-Layer Meteorology, 18, 495–527, https://doi.org/10.1007/BF00119502, 1980.

Fierce, L., Riemer, N., and Bond, T. C.: When is cloud condensation nuclei activity sensitive to particle characteristics at emission?, Journal of Geophysical Research: Atmospheres, 118, 13,476–13,488, https://doi.org/10.1002/2013JD020608, _eprint: https://onlinelibrary.wiley.com/doi/pdf/10.1002/2013JD020608, 2013.

Fierce, L., Riemer, N., and Bond, T. C.: Explaining variance in black carbon's aging timescale, Atmospheric Chemistry and Physics, 15, 3173–3191, https://doi.org/10.5194/acp-15-3173-2015, publisher: Copernicus GmbH, 2015.

Fierce, L., Yao, Y., Easter, R., Ma, P.-L., Sun, J., Wan, H., and Zhang, K.: Quantifying structural errors in cloud condensation nuclei activity from reduced representation of aerosol size distributions, Journal of Aerosol Science, 181, 106 388, https://doi.org/10.1016/j.jaerosci.2024.106388, 2024.

Forster, P., Storelvmo, T., Armour, K., Collins, W., Dufresne, J.-L., Frame, D., Lunt, D., Mauritsen, T., Palmer, M., Watanabe, M., Wild, M., and Zhang, H.: The Earth's Energy Budget, Climate Feedbacks, and Climate Sensitivity, p. 923–1054, Cambridge University Press, Cambridge, United Kingdom and New York, NY, USA, https://doi.org/10.1017/9781009157896.009, 2021.

Golaz, J., Van Roekel, L. P., Zheng, X., Roberts, A. F., Wolfe, J. D., Lin, W., Bradley, A. M., Tang, Q., Maltrud, M. E., Forsyth, R. M., Zhang, C., Zhou, T., Zhang, K., Zender, C. S., Wu, M., Wang, H., Turner, A. K., Singh, B., Richter, J. H., Qin, Y., Petersen, M. R., Mametjanov, A., Ma, P., Larson, V. E., Krishna, J., Keen, N. D., Jeffery, N., Hunke, E. C., Hannah, W. M., Guba, O., Griffin, B. M., Feng, Y., Engwirda, D., Di Vittorio, A. V., Dang, C., Conlon, L. M., Chen, C., Brunke, M. A., Bisht, G., Benedict, J. J., Asay-Davis, X. S., Zhang, Y., Zhang, M., Zeng, X., Xie, S., Wolfram, P. J., Vo, T., Veneziani, M., Tesfa, T. K., Sreepathi, S., Salinger, A. G., Reeves Eyre, J. E. J., Prather, M. J., Mahajan, S., Li, Q., Jones, P. W., Jacob, R. L., Huebler, G. W., Huang, X., Hillman, B. R., Harrop, B. E., Foucar, J. G., Fang, Y., Comeau, D. S., Caldwell, P. M., Bartoletti, T., Balaguru, K., Taylor, M. A., McCoy, R. B., Leung, L. R., and Bader, D. C.: The DOE

E3SM Model Version 2: Overview of the Physical Model and Initial Model Evaluation, Journal of Advances in Modeling Earth Systems, 14, e2022MS003 156, https://doi.org/10.1029/2022MS003156, 2022.

Gustafson Jr., W. I., Qian, Y., and Fast, J. D.: Downscaling aerosols and the impact of neglected subgrid processes on direct aerosol radiative forcing for a representative global climate model grid spacing, Journal of Geophysical Research: Atmospheres, 116, https://doi.org/10.1029/2010JD015480, 2011.

Kaser, L., Karl, T., Yuan, B., Mauldin III, R. L., Cantrell, C. A., Guenther, A. B., Patton, E. G., Weinheimer, A. J., Knote, C., Orlando, J., Emmons, L., Apel, E., Hornbrook, R., Shertz, S., Ullmann, K., Hall, S., Graus, M., de Gouw, J., Zhou, X., and Ye, C.: Chemistry-turbulence interactions and mesoscale variability influence the cleansing efficiency of the atmosphere, Geophysical Research Letters, 42, 10,894–10,903, https://doi.org/10.1002/2015GL066641, _eprint: https://onlinelibrary.wiley.com/doi/pdf/10.1002/2015GL066641, 2015.

Kokkola, H., Korhonen, H., Lehtinen, K. E. J., Makkonen, R., Asmi, A., Järvenoja, S., Anttila, T., Partanen, A.-I., Kulmala, M., Järvinen, H., Laaksonen, A., and Kerminen, V.-M.: SALSA – a Sectional Aerosol module for Large Scale Applications, Atmospheric Chemistry and Physics, 8, 2469–2483, https://doi.org/10.5194/acp-8-2469-2008, publisher: Copernicus GmbH, 2008.

Kurppa, M., Hellsten, A., Roldin, P., Kokkola, H., Tonttila, J., Auvinen, M., Kent, C., Kumar, P., Maronga, B., and Järvi, L.: Implementation of the sectional aerosol module SALSA2.0 into the PALM model system 6.0: model development and first evaluation, Geoscientific Model Development, 12, 1403–1422, https://doi.org/10.5194/gmd-12-1403-2019, publisher: Copernicus GmbH, 2019.

Lin, G., Qian, Y., Yan, H., Zhao, C., Ghan, S. J., Easter, R., and Zhang, K.: Quantification of marine aerosol subgrid variability and its correlation with clouds based on high-resolution regional modeling, Journal of Geophysical Research: Atmospheres, 122, 6329–6346, https://doi.org/10.1002/2017JD026567, 2017.

Ma, P.-L., Rasch, P. J., Wang, M., Wang, H., Ghan, S. J., Easter, R. C., Gustafson Jr., W. I., Liu, X., Zhang, Y., and Ma, H.-Y.: How does increasing horizontal resolution in a global climate model improve the simulation of aerosol-cloud interactions?, Geophysical Research Letters, 42, 5058–5065, https://doi.org/10.1002/2015GL064183, _eprint: https://onlinelibrary.wiley.com/doi/pdf/10.1002/2015GL064183, 2015.

Mohebalhojeh, M., Frederick, S., Riemer, N., and West, M.: A Measure of Spatial Heterogeneity, (in prep), 2024.

Ouwersloot, H. G., Vilà-Guerau de Arellano, J., van Heerwaarden, C. C., Ganzeveld, L. N., Krol, M. C., and Lelieveld, J.: On the segregation of chemical species in a clear boundary layer over heterogeneous land surfaces, Atmospheric Chemistry and Physics, 11, 10 681–10 704, https://doi.org/10.5194/acp-11-10681-2011, publisher: Copernicus GmbH, 2011.

Qian, Y., Gustafson, W. I. J., and Fast, J. D.: An investigation of the sub-grid variability of trace gases and aerosols for global climate modeling, Atmospheric Chemistry and Physics, 10, 6917–6946, https://doi.org/10.5194/acp-10-6917-2010, publisher: Copernicus GmbH, 2010.

Riemer, N., West, M., Zaveri, R. A., and Easter, R. C.: Simulating the evolution of soot mixing state with a particle-resolved aerosol model, Journal of Geophysical Research: Atmospheres, 114, https://doi.org/10.1029/2008JD011073, 2009.

Skamarock, C., Klemp, B., Dudhia, J., Gill, O., Barker, D., Duda, G., Huang, X.-y., Wang, W., and Powers, G.: A Description of the Advanced Research WRF Version 3, https://doi.org/10.5065/D68S4MVH, 2008.

Tilmes, S., Mills, M. J., Zhu, Y., Bardeen, C. G., Vitt, F., Yu, P., Fillmore, D., Liu, X., Toon, B., and Deshler, T.: Description and performance of a sectional aerosol microphysical model in the Community Earth System Model (CESM2), Geoscientific Model Development, 16, 6087–6125, https://doi.org/10.5194/gmd-16-6087-2023, publisher: Copernicus GmbH, 2023.

410 Tonttila, J., Maalick, Z., Raatikainen, T., Kokkola, H., Kühn, T., and Romakkaniemi, S.: UCLALES–SALSA v1.0: a large-eddy model with interactive sectional microphysics for aerosol, clouds and precipitation, Geoscientific Model Development, 10, 169–188, https://doi.org/10.5194/gmd-10-169-2017, publisher: Copernicus GmbH, 2017.

Vignati, E., Wilson, J., and Stier, P.: M7: An efficient size-resolved aerosol microphysics module for large-scale aerosol transport models, Journal of Geophysical Research: Atmospheres, 109, https://doi.org/10.1029/2003JD004485, _eprint: 415 https://onlinelibrary.wiley.com/doi/pdf/10.1029/2003JD004485, 2004.

Weigum, N., Schutgens, N., and Stier, P.: Effect of aerosol subgrid variability on aerosol optical depth and cloud condensation nuclei: implications for global aerosol modelling, Atmospheric Chemistry and Physics, 16, 13 619–13 639, https://doi.org/10.5194/acp-16-13619-2016, publisher: Copernicus GmbH, 2016.

Zaveri, R. A. and Peters, L. K.: A new lumped structure photochemical mechanism for large-scale applications, Journal of Geophysical 420 Research: Atmospheres, 104, 30 387–30 415, https://doi.org/10.1029/1999JD900876, 1999.

Zaveri, R. A., Easter, R. C., and Peters, L. K.: A computationally efficient Multicomponent Equilibrium Solver for Aerosols (MESA), Journal of Geophysical Research: Atmospheres, 110, https://doi.org/10.1029/2004JD005618, 2005a.

Zaveri, R. A., Easter, R. C., and Wexler, A. S.: A new method for multicomponent activity coefficients of electrolytes in aqueous atmospheric aerosols, Journal of Geophysical Research: Atmospheres, 110, https://doi.org/10.1029/2004JD004681, _eprint: 425 https://onlinelibrary.wiley.com/doi/pdf/10.1029/2004JD004681, 2005b.

Zaveri, R. A., Easter, R. C., Fast, J. D., and Peters, L. K.: Model for Simulating Aerosol Interactions and Chemistry (MOSAIC), Journal of Geophysical Research: Atmospheres, 113, https://doi.org/10.1029/2007JD008782, 2008.

Zaveri, R. A., Barnard, J. C., Easter, R. C., Riemer, N., and West, M.: Particle-resolved simulation of aerosol size, composition, mixing state, and the associated optical and cloud condensation nuclei activation properties in an evolving urban plume, Journal of Geophysical 430 Research: Atmospheres, 115, https://doi.org/10.1029/2009JD013616, 2010.